metals

MDPI

Article

Increase in the Mechanical Strength of Mg-8Gd-3Y-1Zn Alloy Containing Long-Period Stacking Ordered Phases Using Equal Channel Angular Pressing Processing

Gerardo Garces [1,*], Pablo Pérez [1], Rafael Barea [2], Judit Medina [1], Andreas Stark [3], Norbert Schell [4] and Paloma Adeva [1]

1 Departamento de Metalurgia Física, Centro Nacional de Investigaciones Metalúrgicas, CENIM, CSIC, Avda. Gregorio del Amo 8, 28040 Madrid, Spain; zubiaur@cenim.csic.es (P.P.); judit.medina@cenim.csic.es (J.M.); adeva@cenim.csic.es (P.A.)

2 Departamento de Ingeniería Industrial, Universidad Nebrija, Campus Dehesa de la Villa, C. Pirineos 55, 28040 Madrid, Spain; rbarea@nebrija.es

3 Institute of Materials Research, Helmholtz-Zentrum Geesthacht, Max-Planck-Str. 1, 21502 Geesthacht, Germany; Andreas.Stark@hzg.de

4 Structural Research on New Materials, Helmholtz-Zentrum Geesthacht, Outstation at DESY, Notkestraße 85, 22607 Hamburg, Germany; norbert.schell@hzg.de

* Correspondence: ggarces@cenim.csic.es; Tel.: +34-91-5538900 (ext. 336)

Received: 11 January 2019; Accepted: 1 February 2019; Published: 13 February 2019

Abstract: The evolution of the microstructure and mechanical properties during equal channel angular pressing processing has been studied in an extruded Mg-Gd-Y-Zn alloy containing long-period stacking ordered phases. After extrusion, the microstructure is characterized by the presence of long-period stacking ordered fibers elongated along the extrusion direction within the magnesium matrix. The grain structure is a mixture of randomly oriented dynamic recrystallized and coarse highly oriented non-dynamic recrystallized grains. Rare-earth atoms are in solid solution after extrusion at 400 °C and precipitation takes place during the thermal treatment at 200 °C. Precipitation of β′ prismatic plates and lamellar γ′ in the basal plane increases the tensile yield stress from 325 to 409 MPa. During equal channel angular pressing processing at 300 °C, the volume fraction of dynamic recrystallized grains continuously increases with the strain introduced during the equal channel angular pressing process. Precipitation of β phase is equally observed at grain boundaries of the ECAPed alloy. Dynamic recrystallized grain size decreases from 1.8 μm in the extruded material to 0.5 μm in the ECAPed alloy. Thermal treatment at 200 °C of ECAPed materials results in an increase of the yield stress up to 456 MPa, which is maintained up to 200 °C.

Keywords: magnesium alloys; LPSO; ECAP; precipitation

1. Introduction

Extruded Mg-RE-Zn alloys containing Long-Period Stacking Ordered (LPSO) phases exhibit a high mechanical strength near 400 MPa, with appreciable ductility [1–4]. The microstructure of these alloys consists of LPSO-phase fibers elongated along the extrusion direction in a non-fully recrystallized magnesium matrix. Most of studies on this kind of alloy have been carried out in the Mg-Y-Zn system. However, it has been proved that the addition of Gd to the alloys of this system is very interesting since the alloys combine a high mechanical strength (higher than 400 MPa) and high elongation to failure (around 15%) [5–13]. Extruded or hot-rolled alloys exhibit a bimodal grain structure with fine

dynamic recrystallized (DRXed) grains and coarse non-DRXed grains highly oriented with the basal plane parallel to the extrusion direction. This heterogeneous microstructure induces some interesting mechanical characteristics in material. The strengthening of the alloy has been analyzed in terms of a composite consisting of a bimodal grain-structured magnesium matrix and fiber-shaped LPSO phase particles. Thus, a large fraction of randomly oriented recrystallized grains increases ductility, while large areas of deformed grains with a strong texture characterized by the basal planes parallel to the extrusion or rolling directions provoke an increase of the strength. Moreover, these alloys are susceptible to age-hardening due to the precipitation of β′ plates in the prismatic planes.

The main reinforcing mechanism of Mg-Gd-Y-Zn alloys is the refinement of the grain size, which can be magnified by the use of severe plastic deformation (SPD) methods. High pressure torsion (HPT) was successfully used in Mg-Gd-Y-Zn alloys for obtaining nano-sized grains with high-angle misorientations with ultra-high hardness values [12,13]. However, HPT samples are normally small for industrial applications. Equal Channel Angular Processing (ECAP) constitutes an alternative SPD method to produce an ultrafine microstructure in magnesium alloys. In Mg-Y-Zn alloys containing LPSO-phases, ECAP processing not only decreases the grain size of DRXed grains, but also promotes an increase in the volume fraction of these DRXed grains as the accumulated strain is increased [14,15].

This study explores the use of ECAP processing in an extruded and age-hardening Mg-Gd-Y-Zn alloy containing LPSO phases. The changes in the microstructure and mechanical properties will be evaluated during ECAP processing using electron microscopy, synchrotron radiation diffraction (SDR), and tensile tests.

2. Materials and Methods

The Mg-8Gd-3Y-1Zn (wt.%) alloy (designed as GWZ831) was prepared with high purity pure Mg, Zn, and Mg-20%Gd and Mg-22%Y master alloys by melting and casting. The cast ingot was homogenized at 560 °C for 24 h (designated as solution heat treatment), quenched in water, and subsequently machined as cylinders with a 41 mm diameter and 200 mm length. The cylinders were extruded at 400 °C with an extrusion ratio of 4:1. Then, cylinders of a 70 mm length and 20 mm of diameter were ECAP processed at 300 °C using the route A. The angle of the ECAP was 118°, which produces a true strain of 0.7 per pass. Samples were heated in the die and the ECAP rate speed used in all cases was 20 mm/min. The cylinders were processed up to four and six passes, without internal damage. After each ECAP pass, the sample was quenched in water. Samples after extrusion and ECAP processing were aged during 24 h at 200 °C (designated as peak-aged condition), following previous studies [5,7–9].

Synchrotron radiation diffraction (SRD) experiments were carried out on the P07B beamline of PETRA III, at the Deutsches-Elektronen-Synchrotron (DESY, Hamburg, Germany), to identify the different phases presented in the alloy in the as-extruded condition, as well as after thermal treatments and/or the ECAP processing. The gauge volume was $1 \times 1 \times 5$ mm^3 (beam section x cylinder diameter). The diffraction patterns were recorded by a Perkin-Elmer XRD 1622 flat panel detector with an array of 2048^2 pixels, with an effective pixel size of 200×200 μm^2. The wavelength of the beam was 0.01423 nm. LaB6 was used as a reference to calibrate the acquired diffraction pattern. The detector-to-sample distance was 1616.5 mm. Conventional 2θ diffraction profiles were obtained by azimuthal integration of the Debye-Scherrer rings in the axial and radial direction using the FIT2D (Grenoble, France) software [16].

Microstructural characterization was carried out by scanning and transmission electron microscopy (SEM and TEM, respectively), as well as by the Electron Backscattered Diffraction (EBSD) technique attached to SEM.

SEM samples were prepared by conventional polishing and finishing, with an etching solution of 5 mL acetic acid, 20 mL water, and 25 mL picric acid in methanol. Quantitative image analysis was carried out to measure the recrystallized fraction and grain size in the magnesium matrix. In order to obtain good statistical values, 10 SEM images and 500 grains were measured.

The texture of the processed alloy was measured using the Electron back-scattered diffraction technique (EBSD) technique. Since samples have a cylindrical symmetry, two reference directions: ED

(extrusion direction) and RD (radial direction), were selected. Specimens for EBSD measurements were polished with a solution of alumina in distilled water and finally chemically etched with a cold solution of 7 mL of acetic acid, 3 mL of nitric acid, 30 mL of ethanol, and 10 mL of water.

TEM has been carried out to analyze precipitates presented in the samples after ECAP processing, as well as after the second thermal treatment. Specimens for TEM were prepared by electrolytic polishing using a reactive mixture of 25% nitric acid and 75% methanol at −30 °C and 25 V. Then, ion milling at liquid nitrogen temperature was used to remove the fine oxide film formed on the surface during electrolytic polishing.

The mechanical properties of the extruded alloy after ECAP processing were evaluated by tensile testing cylindrical samples with a diameter of 3 mm and gauge length of 10 mm. Tensile tests were carried out using a universal testing machine at a strain rate of 4×10^{-4} s^{-1} from room temperature up to 200 °C. All tensile samples were tested along the extrusion or ECAP directions.

3. Results

Figure 1 is a backscattered electron image showing the microstructure of the as-cast GWZ831 alloy after solubilization treatment. Two phases are clearly observed: The magnesium phase (dark phase) and the LPSO phase (white phase). The volume fraction of the LPSO phase is 11%. After the extrusion (hereinafter the material in the as-extrusion condition will also be designated as 0 ECAP passes), the LPSO phase is deformed and elongated along the extrusion direction (Figure 2a). The magnesium matrix exhibits a bimodal grain structure constituted of areas of coarse non-DRXed grains elongated along the extrusion direction with a length between 50–100 μm and areas of fine equiaxed DRXed grains (Figure 2b). The volume fractions of non-DRXed and DRXed grains areas are 47 and 42%, respectively (Figure 3). The average grain size of DRXed grains is 1.8 μm (Figure 4 (top)).

The volume fraction and grain size of DRXed grains experience significant changes with the number of ECAP passes (Figure 2c–f). Thus, the volume fraction of DRXed grain areas becomes 71% after six ECAP passes (Figure 3), while the grain size is gradually refined to 0.5 and 0.6 μm after four and six ECAP passes, respectively (Figure 4). Furthermore, small particles precipitate at grain boundaries of DRXed grains after four and six ECAP passes (Figure 2d,f). Such particles, however, are absent within the coarse grains.

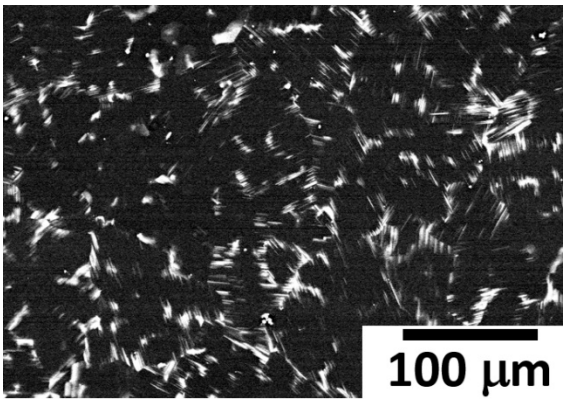

Figure 1. Back-scattered image of the as-cast GWZ31alloy.

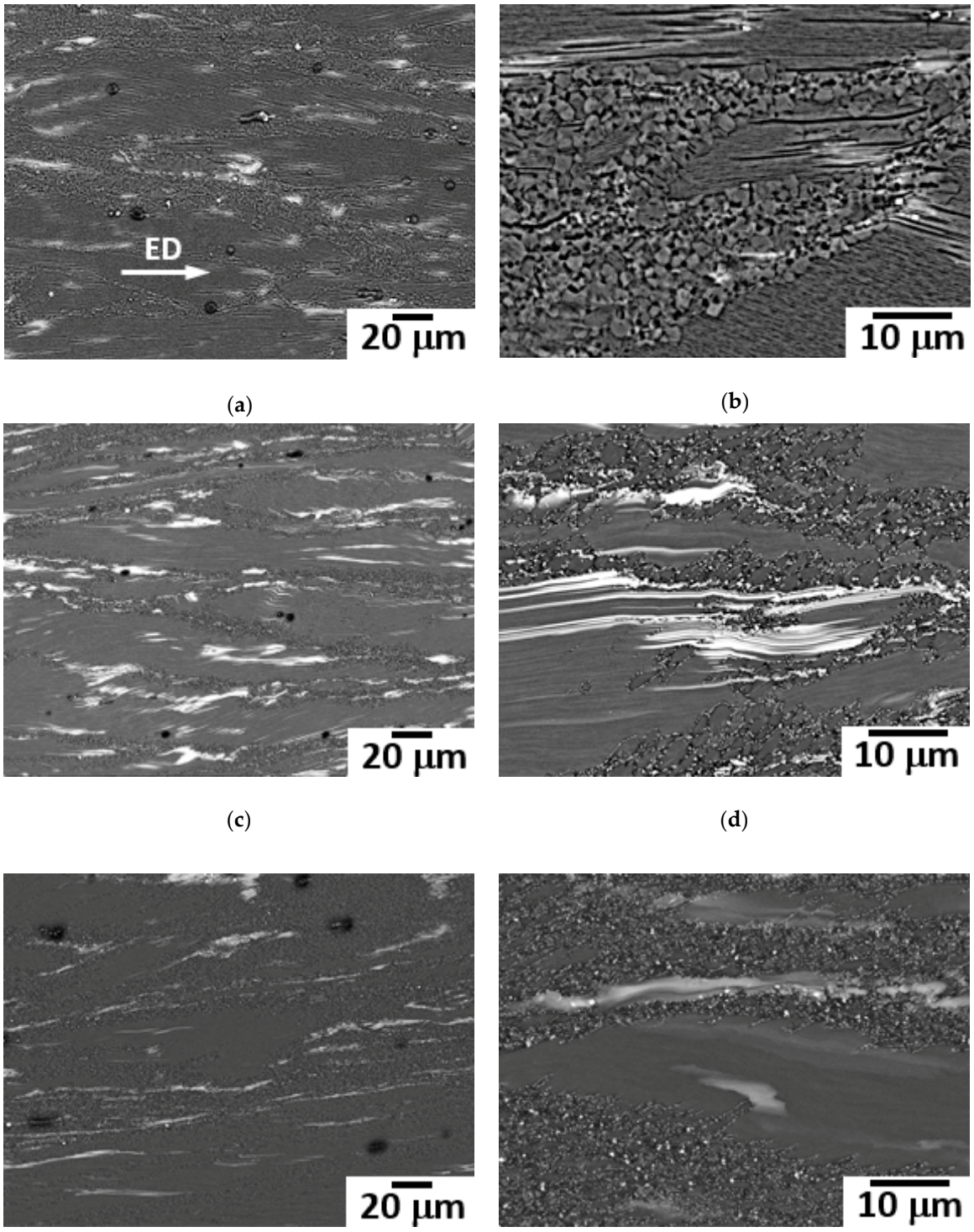

Figure 2. T Back-scattered image of the extruded GWZ31 alloy along the extrusion or ECAP directions after (**a**,**b**) 0, (**c**,**d**) 4, and (**e**,**f**) 6 ECAP passes. (The white arrow indicates the extrusion or ECAP direction).

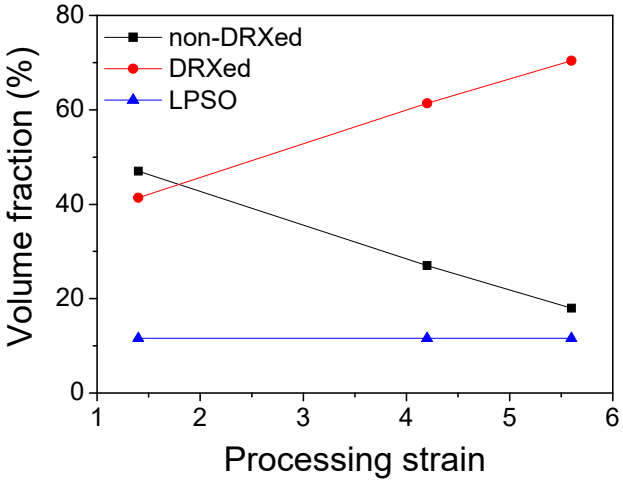

Figure 3. Evolution of the volume fraction of LPSO phase, DRXed grains, and non-DRXed grains as a function of the processing strain.

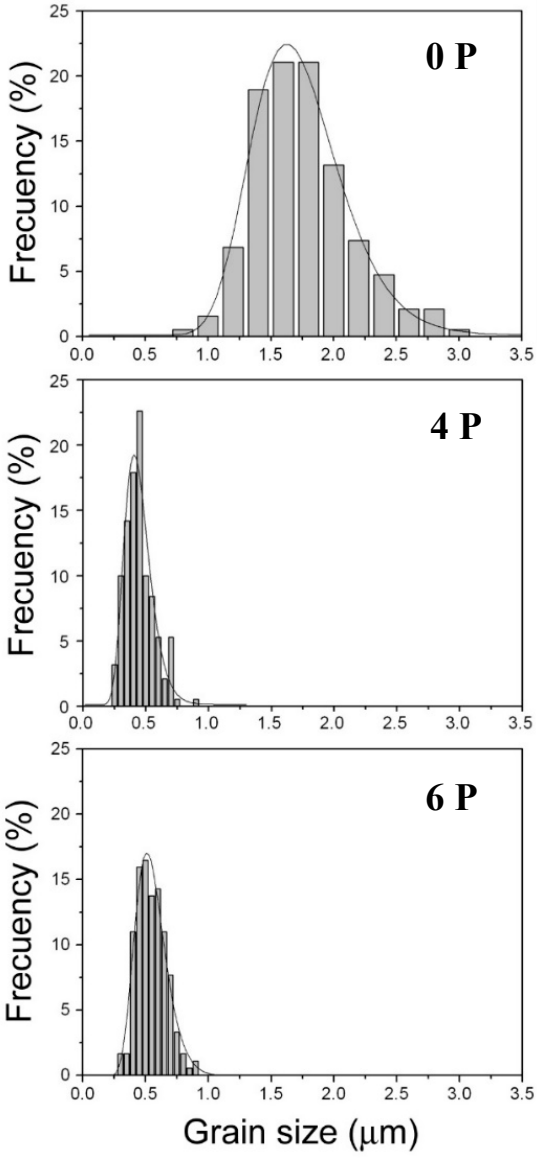

Figure 4. Histograms of grain size of the extruded GWZ31 alloy after 0, 4, and 6 ECAP passes.

The orientation image mappings (OIM) of the magnesium grains (Figure 5a–e) and the {10$\bar{1}$0} pole figures obtained from the OIM image (Figure 6a–e) in the extruded alloy and after four and six ECAP passes reveal significant changes induced by the high strain introduced during the ECAP processing. In the case of the material after ECAP processing, two images were shown due to the high difference in grain size between DRXed and non-DRXed grains. DRXed grains are randomly oriented, while non-DRXed grains are highly oriented, with their basal planes parallel to the extrusion direction (see Figure 6). It is important to point out that areas of non-DRXed grains are deformed during ECAP processing and local misorientations are observed within these grains (Figure 5c,e).

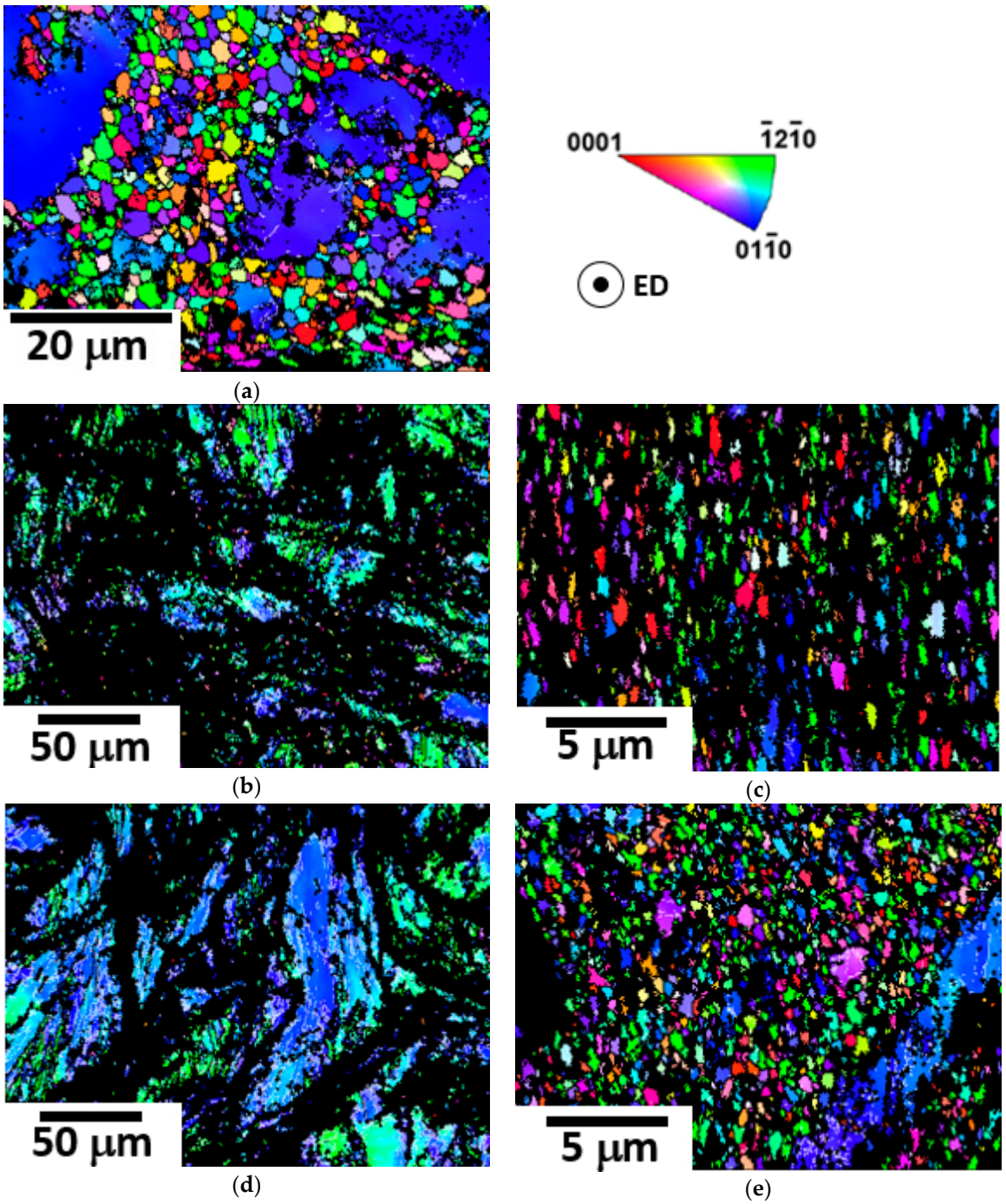

Figure 5. Orientation Image Mapping of the extruded GWZ831 alloy after (**a**) 0, (**b**,**c**) 4, and (**d**,**e**) 6 ECAP passes. Extrusion or ECAP direction is perpendicular to the image.

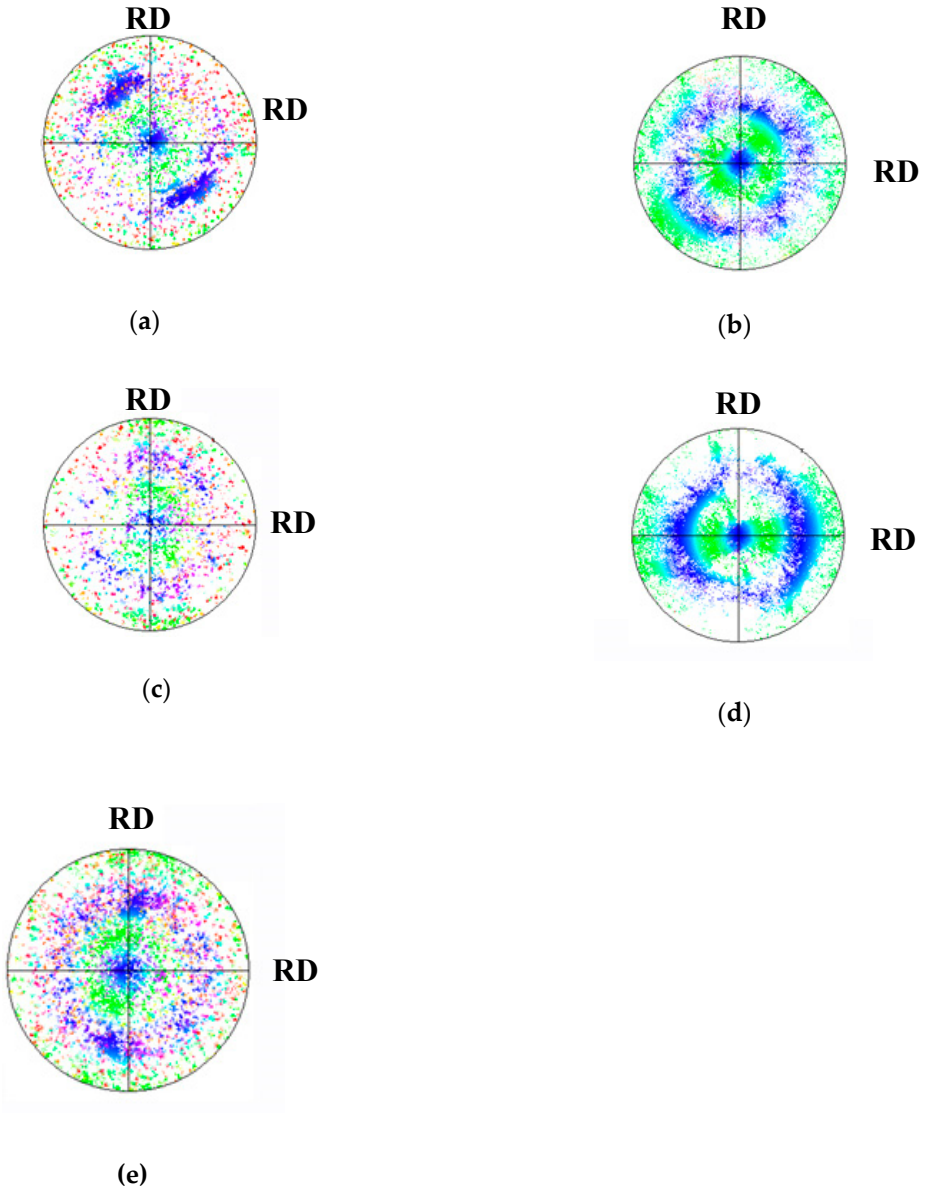

Figure 6. {10$\bar{1}$0} pole figures obtained from the EBSD image of Figure 5 of the extruded GWZ831 alloy after (**a**) 0, (**b**,**c**) 4, and (**d**,**e**) 6 ECAP passes. Extrusion or ECAP direction is perpendicular to the image.

Figure 7 shows TEM images of equiaxed DRXed grains (Figure 7a), coarse non-DRXed grains (Figure 7b), and LPSO phase (Figure 7c) of the material in the extrusion condition. It is interesting to note the presence within the magnesium grains, especially in coarse non-DRXed grains, of thin lamellae parallel to basal planes. These lamellae produce the diffuse streaks along the [0002] direction in the selected area diffraction pattern (SADP) of Figure 7b. A high dislocation density is observed in non-DRXed grains areas. Figure 7c shows a bright field TEM image of the elongated LPSO fiber along the extrusion direction. Moreover, the SADP of the LPSO phase in the [11$\bar{2}$0] zone axis shows that the crystallographic lattice structure corresponds to the 14H. Figure 8 shows the TEM images of non-DRXed (a,c) and DRXed (b,d) areas after four and six ECAP passes. A very fine grain size in the DRXed grain areas is observed, in agreement with the SEM images of Figure 2. Moreover, the presence of particles of 100 nm is noticed at grain boundaries in the DRXed grains (Figure 7e). In the case of coarse DRXed grains, these particles are only found within the grain after six passes of ECAP. SADP analysis of these particles reveals that they correspond to β particles with a lattice parameter of 2.23 nm. As an example, the SAPD in the [111] zone axis is presented in Figure 8f. Since these precipitates

were not present in the extruded material, it can be assumed that the precipitation occurred during ECAP processing at 300 °C. Accordingly, some gadolinium and yttrium atoms remain in solid solution during the extrusion process and only after thermal treatment at 200 °C for 24 h are fine precipitates observed in the as-extruded alloy, as shown in Figure 9, where precipitates in the [11$\bar{2}$0] zone axis are displayed. These observations are in good agreement with previous studies, given that a high density of prismatic plate β′-precipitates with a base-centered orthorhombic structure is observed [5,7–9].

The precipitation process during the ECAP processing, as well as the formation of β′-precipitates, has been studied by SRD. Figure 10 shows the Debye-Scherrer rings obtained in the as-extruded alloy and after four and six ECAP passes. After integration along the axial and radial directions, diffraction patterns as a function of 2θ can be obtained. Figure 11a shows the axial and radial diffraction pattern of the as-extruded alloy. Owing to the intense fiber texture of the non-DRXed grains, observed in Figure 6, the diffraction peak corresponding to the {10$\bar{1}$0} planes exhibits the highest intensity in the axial direction and the diffraction peak corresponding to the {0002} planes exhibits the highest intensity in the radial direction. The presence of an intense diffraction peak is only observed in the radial direction at 2θ = 0.45°, which corresponds to the (0002) diffraction peak of the 14H LPSO-phase crystal structure. The LPSO-phase fibers are equally highly oriented, with the basal plane parallel to the extrusion direction.

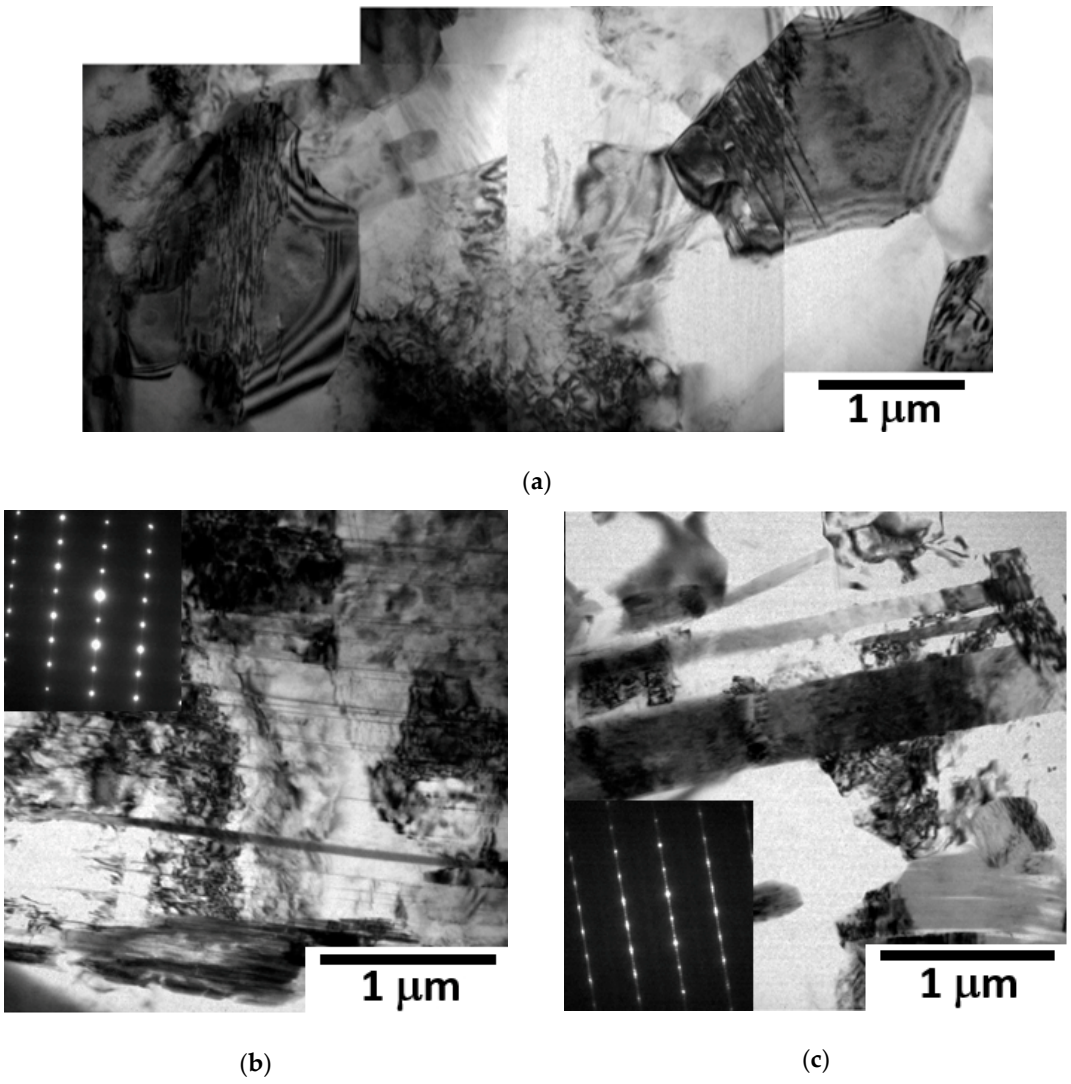

(**a**)

(**b**) (**c**)

Figure 7. Bright field TEM images and SAED pattern of the extruded GWZ831 alloy of the (**a**) DRXed grains, (**b**) non-DRXed grains (B = [11$\bar{2}$0]), and (**c**) LPSO phase (B = [11$\bar{2}$0]).

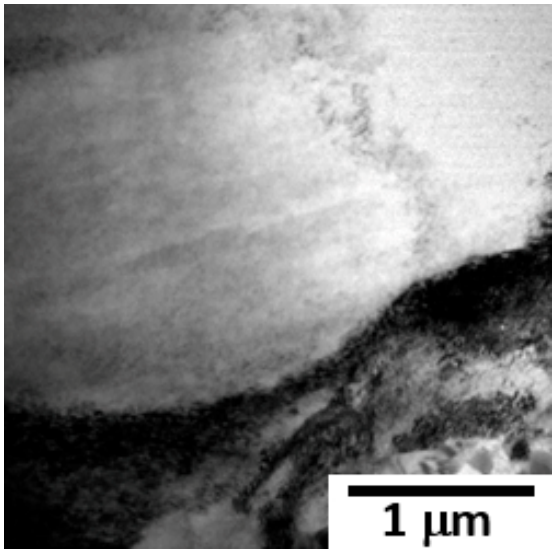

(**a**)

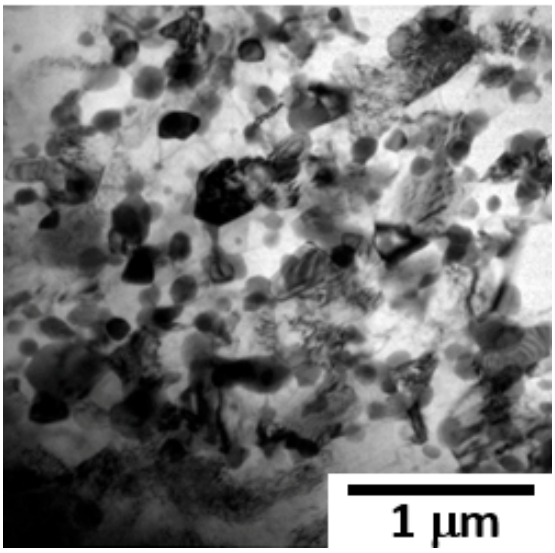

(**b**)

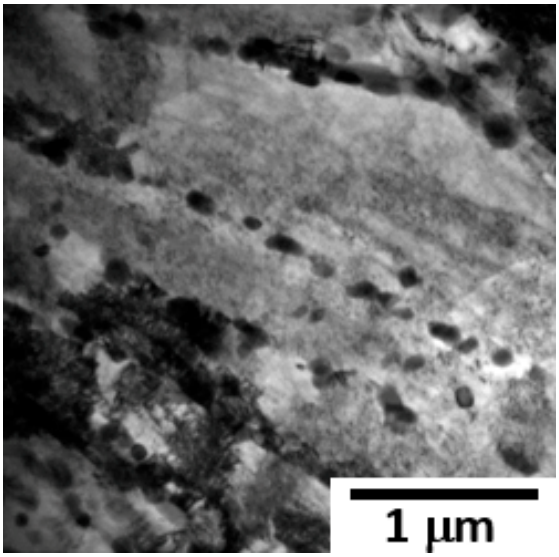

(**c**)

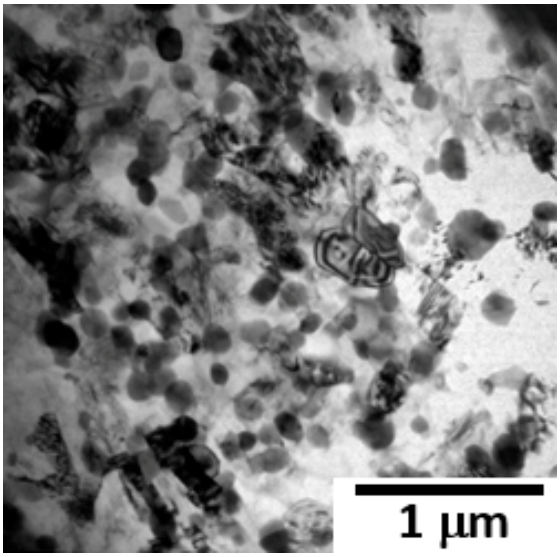

(**d**)

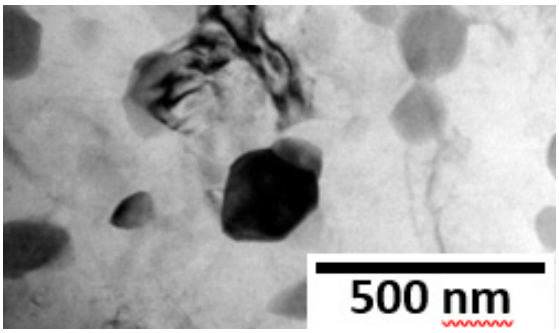

(**e**)

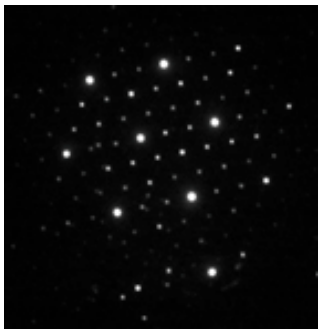

(**f**)

Figure 8. Bright field TEM images of the extruded GWZ831 alloy after (**a**,**b**) 4 and (**c**,**d**) 6 ECAP passes. a and c images correspond to non-DRXed grains and b and d images correspond to DRXed grains. (**e**) TEM images and (**f**) SAED pattern of β particles (B = [111]).

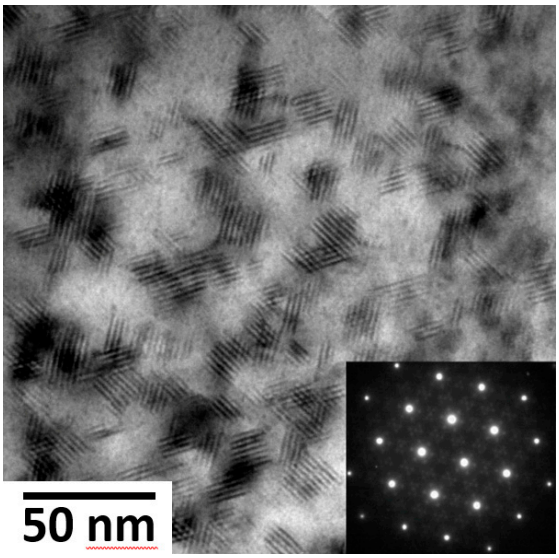

Figure 9. Bright field TEM image and SAED pattern of the extruded GWZ831 alloy aged 24 h at 200 °C, showing the β′ precipitates lying on the prismatic plane (B = [0002]).

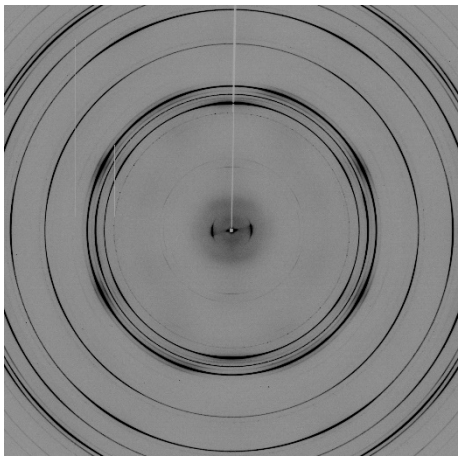

(**a**)

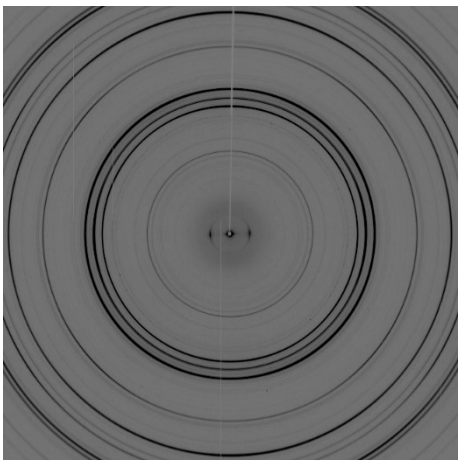

(**b**)

Figure 10. *Cont*.

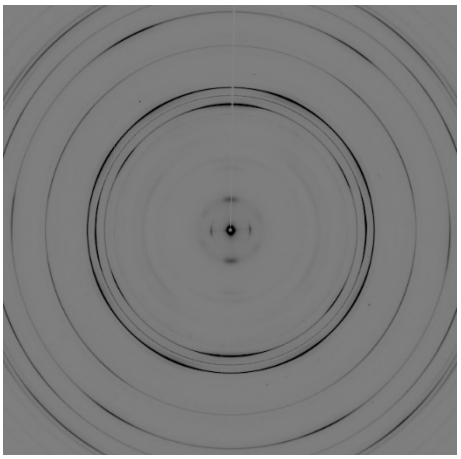

(**c**)

Figure 10. Synchrotron diffraction pattern recorded on the 2D flat-panel detector of the extruded GWZ831 alloy after (**a**) 0, (**b**) 4, and (**c**) 6 ECAP passes.

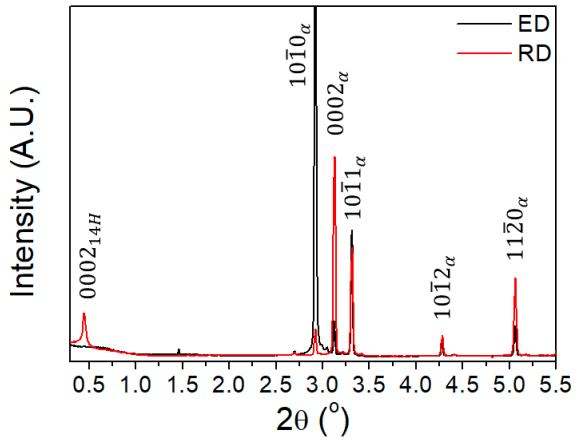

(**a**)

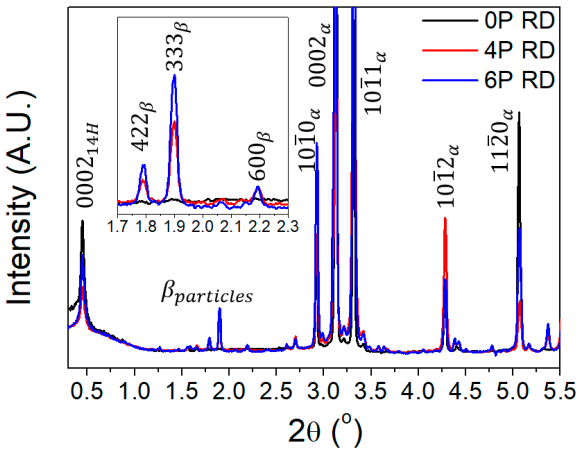

(**b**)

Figure 11. *Cont.*

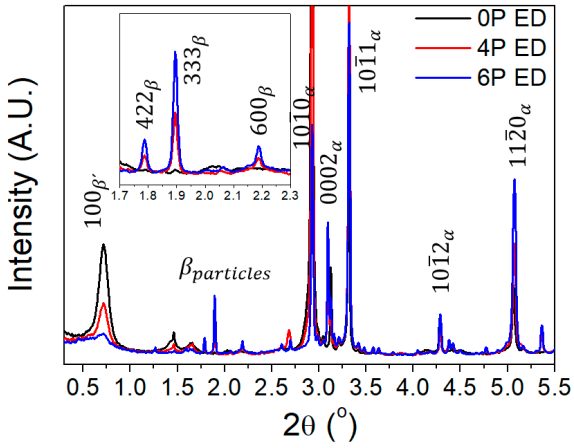

(**c**)

Figure 11. (**a**) Axial and radial diffraction patterns as a function of 2θ obtained by integration of the Debye-Scherrer diffraction rings for the as-extruded alloy. (**b**) Radial diffraction patterns as a function of 2θ obtained by integration of the Debye-Scherrer diffraction rings for the as-extruded alloy and after ECAP processing. (**c**) Axial diffraction patterns as a function of 2θ obtained by integration of the Debye-Scherrer diffraction rings for the as-extruded alloy and after ECAP processing aged at 200 °C for 24 h.

Figure 11b shows the radial diffraction patterns of the GWZ831 alloy after extrusion and after four and six ECAP passes at 300 °C. In Figure 11b, a detail of the diffraction patterns' diffraction angles, θ, between 1.7 and 2.3°, is presented. New diffraction peaks corresponding to the β phase are observed, in agreement with TEM images, only after ECAP processing.

Finally, Figure 11c shows the axial diffraction patterns of the GWZ831 alloy after extrusion (0 ECAP passes) and after four and six ECAP passes at 300 °C and thermal treatment at 200 °C for 24 h. An additional peak is observed at 2θ = 0.72°, which corresponds to the (020) plane of the β′-precipitates. The intensity of the (020) diffracted peak decreases with the increase of the processing strain. Even after six ECAP passes, the diffraction peaks almost disappear due to the magnesium matrix being almost free of alloying elements in solid solution and only transformation of β′ in β is taking place, as deduced from the increase of the intensity peaks associated with β phase. Honna et al. reported [5] that the orientation relationship with the magnesium matrix is $(001)_{\beta'}//(0001)_\alpha$ and $[100]_{\beta'}//[2\bar{1}\bar{1}0]_\alpha$. Therefore, this peak corresponds to β′ precipitates, mainly located in the non-DRXed grains. The decrease in the volume fraction of non-DRXed grains as a function of the processing strain can also decrease the (020) diffraction peak of β' precipitates.

The influence of the ECAP processing and the thermal treatment of aging on the mechanical properties has been evaluated through tensile tests (Figure 12a). The mechanical strength increases with the processing strain (Figure 12b), but the opposite is true for the elongation to failure (from 7.5% for the extruded alloy to 3.5% after six ECAP passes). Annealing at 200 °C for 24 h produced an additional increase in the yield stress of around 100 MPa, reaching 454 and 456 MPa for the alloy after four and six ECAP passes, respectively. It is interesting to point out that after this aging treatment, the mechanical strength of the alloy is even higher than after the ECAP processing. This behavior is maintained up to 200 °C, where the GWZ831 alloy processed using an ECAP route exhibits a yield stress close to 400 MPa. Above this temperature, the mechanical strength of the alloy falls abruptly, with the yield stress of ECAPed samples remaining below that of the extruded alloy (Figure 12c). At 300 °C, elongation to failure increases up to 39, 65, and 61% for the extruded alloy and the extruded alloy after four and six ECAP passes, respectively.

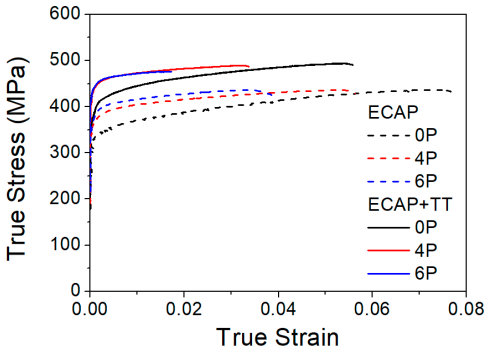

(**a**)

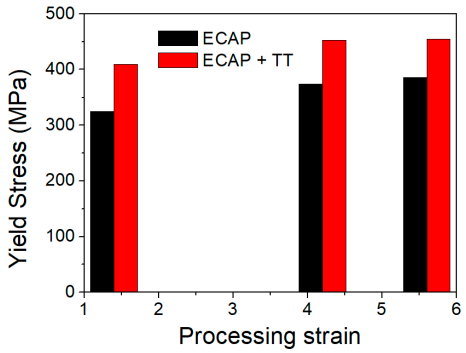

(**b**)

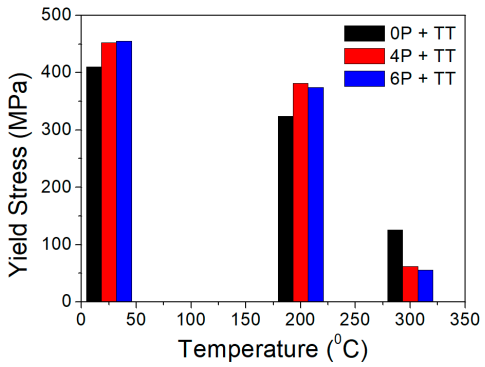

(**c**)

Figure 12. (**a**) Tensile macroscopic stress-strain curve of the GWZ831 alloy for the as-extruded alloy and after ECAP processing with/without thermal treatment at 200 °C for 24 h. (**b**) Evolution of the yield stress as a function of the processing strain of the GWZ831 alloy for the as-extruded alloy and after ECAP processing with/without thermal treatment at 200 °C for 24 h. (**c**) Evolution of the yield stress as a function of the tensile temperature of the GWZ831 alloy for the as-extruded alloy and after ECAP processing aged at 200 °C for 24 h.

4. Discussion

The results show that the microstructure and, therefore, the properties of the GWZ831 alloy, are very sensitive to the processing route. The volume fraction of DRXed and non-DRXed grains, the grain size, and the coexistence of different types of precipitates depend on the number of passes during ECAP processing, as well as on subsequent ageing treatments. Thus, ageing treatment at

200 °C for 24 h of a sample with six ECAP passes results in an increase of 40% of the mechanical strength compared with the material in the as-extruded condition, (from 325 MPa to 456 MPa). Several reinforcing mechanisms have been proposed to explain the increase in the mechanical strength of Mg-Gd-RE-Zn alloys [4–13], such as grain size refinement, LPSO phase, solid solution, precipitation, dislocation, and nanoscale segregation. Unfortunately, all these parameters change differently during the ECAP processing, and it is not possible to carry out a systematic study to isolate each contribution. Consequently, analysis of the mechanical strength will take into account the contribution of the main mechanisms inducing major hardening, such as grain size, the LPSO phase, and the formation of prismatic β′ precipitates in these alloys. All these contributions are greatly influenced by ECAP processing.

4.1. Grain Refinement

The use of ECAP processing considerably refines the grain size of the extruded alloy, being approximately three times finer. Since the grain size for the alloy ECAP processed after four and six passes is hardly changed, grain size refinement tends to saturate beyond four passes. However, the mechanical strength of the alloys continues to increase with additional ECAP passes because of the gradual increase in the volume fraction of fine equiaxed DRXed grains. The high strength of the alloy after ECAP remains almost constant up to 200 °C, while above this temperature, the strength drops to very small values, which is attributed to the occurrence of the grain boundary sliding (GBS) mechanism [17,18]. However, the elongation to failure in the three materials (0, 4, and 6 passes) is far from 200%, which is considered as the limit to assume superplasticity. Figure 13 shows the OIMs of the tensile sample after tensile deformation at 300 °C after zero and six ECAP passes. It is interesting to point out that the complete dynamic recrystallization was not produced in coarse non-DRXed grains, which complicates superplasticity. GBS can only occur at DRXed grains, explaining the low elongation to failure at 300 °C in this alloy compared with other ultrafine magnesium alloys [17,18].

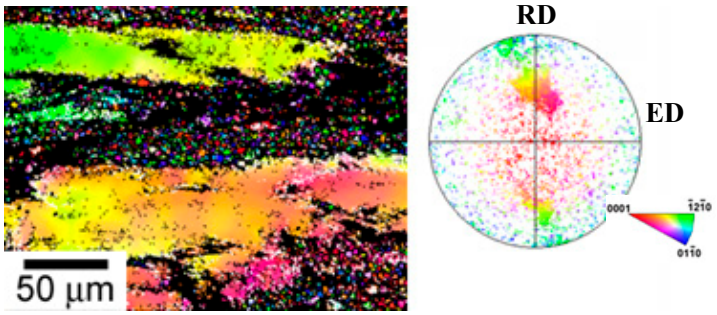

(**a**)

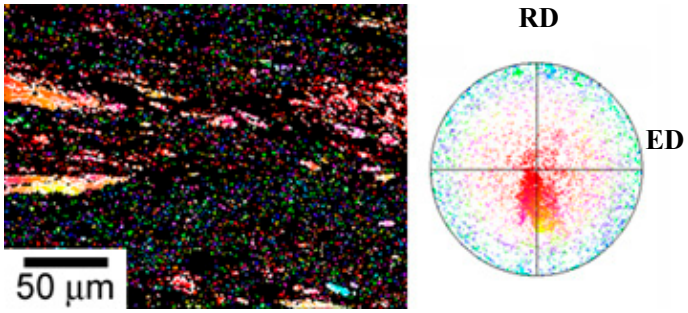

(**b**)

Figure 13. (**a**) Orientation Image Mapping and (0002) pole figure of the deformed samples at 300 °C of the extruded GWZ831 alloy after (**a**) 0 and (**b**) ECAP passes in the peak aged condition. The white arrow indicates the extrusion or ECAP direction.

4.2. LPSO Phase

It is reported that the presence of the LPSO phase improves the mechanical strength of the Mg-RE-Zn alloys [1–4]. On one hand, the LPSO phase, independently of its crystal structure (18R or 14H), has a higher Young modulus than magnesium alloys [19,20], so the magnesium matrix can transfer part of its load to the LPSO phase [21,22]. On the other hand, the resolved shear stress for the basal slip in the LPSO phase is one order of magnitude higher than that in magnesium [23], and its activation is not expected.

It is important to note that the mechanical and plasticity behavior of the LPSO phase are strongly dependent on its crystallographic texture. The LPSO phase in extruded or ECAPed Mg-RE-Zn alloys is oriented with the basal plane parallel to the extrusion or ECAP direction (Figure 6). With this orientation, the activation of basal slip in the tensile sample is forbidden and only kinking (in compression) or non-basal slip is reported [23–25]. Since the intensity of the (0002) diffraction peak in the radial direction is similar in the three materials, no changes in the texture of the LPSO phase were observed during the ECAP processing. Nevertheless, kinking easily visible in LPSO-phase laths suggests that LPSO-phase in ECAPed samples is harder than LPSO-phase in the extruded alloy.

4.3. Precipitation of Prismatic Plates

Yttrium and gadolinium atoms are in solid solution in the extruded alloy. The formation of coherent prismatic β′ plates after annealing at 200 °C increases the yield stress of the extruded alloy, exceeding the yield stress 400 MPa with appreciable ductility. During the ECAP at 300 °C, after four passes, wide precipitation of β particles is noticed at grain boundaries of fine equiaxed DRXed grains, but not within non-DRXed grains (Figura 8a). This indicates that at the ECAP temperature, higher than that of ageing treatment, grain boundaries permit the rapid diffusion of alloying elements in solid solution and their subsequent precipitation as β-phase. The absence of such precipitates inside coarse non-DRXed grains suggests that solid solution is still preserved in these grains, so they could be susceptible to further ageing. Moreover, the precipitation of β′ precipitates can be achieved through the proper choice of ageing conditions. This can be clearly observed in Figure 11 c, where the diffraction peak of the β′ precipitates in non-DRXed grains decreases with the number of ECAP passes. In the material after six ECAP passes, β particles are also observed within non-DRXed grains and the precipitation of β′ plates is not presented. This means that successive passes at the ECAP temperature favor the precipitation of β′-phase and its subsequent transformation into the β-phase.

This fact could not directly explain the increase in the yield stress observed in the three materials with the thermal treatment (Figure 12). If the precipitation of β′-phase as prismatic plates tends to disappear with ECAP processing at 300 °C, the strength due to precipitation also has to decrease dramatically. Experimentally, the increase in the yield stress after thermal treatment slightly decreases from 85 MPa in the as-extruded alloy to 69 MPa after six ECAP passes. On one hand, the diffraction peak corresponding to β′ precipitates in non-DRXed grains does not disappear completely. Moreover, the volume fraction of non-DXRed grains also decreases below half the magnitude measured in the extruded material (Figure 3). Therefore, it could be expected that β′ precipitates are still presented to reinforce the alloy. On the other hand, during ECAP processing, the partial dissolution of the LPSO phase could occur and solute atoms could segregate, during the thermal treatment at 200 °C, in those defects generated during ECAP, such as vacancies or dislocations. Sun et al. [12,13] have demonstrated, using high-angle annular dark-field scanning TEM, the segregation along the grain boundaries of Gd, Y, and Zn atoms during HPT in this alloy. The use of a combination process based on a T6 + HPT + T5 treatment in a similar alloy induces the highest hardness. However, this study is still unclear and the research is still ongoing.

5. Conclusions

The influence of ECAP processing on the microstructure and mechanical properties in an extruded magnesium-rare-earth alloy containing LPSO phases has been studied using electron microscopy, SRD, and tensile tests. The following conclusions can be drawn:

(1) After extrusion at a high temperature, the magnesium alloy is not fully recrystallized, and its grain structure is characterized by fine DRXed grains randomly oriented and coarse non-DRXed grains highly oriented with the basal plane parallel to the extrusion direction;
(2) During ECAP processing, the volume fraction of DRXed grains increases at the expense of non-DRXed grains. The DRXed grain size decreases to around 500 nm. Grain refinement is the main contribution to the reinforcement mechanism of the alloy;
(3) After thermal treatment at 200 °C, the precipitation of β′ in the prismatic planes is developed in the as-extruded alloy. These precipitates highly improve its tensile yield stress. The yield stress values around 450 MPa are attained at room temperature;
(4) During ECAP processing at 300 °C, β particles are formed at grain boundaries, reducing the capacity to precipitate β′ plates in the prismatic planes;
(5) The mechanical strength is maintained up to 200 °C. Above this temperature, the mechanical resistance drastically decreases due to the ultrafine DRXed grains.

Author Contributions: Each author equally contributed to the development of the paper. G.G. and R.B. carried out the processing of the materials and their microstructural characterization. G.G., P.P., and J.M. contributed to the microstructural and mechanical characterization of the materials. A.S and N.S. helped to carry out the synchrotron radiation diffraction experiments at beamline P07, DESY. P.A. contributed to the paper writing and interpretation.

Funding: This research was funded by the Spanish Ministry of Economy and Competitiveness, grant number MAT2016-78850-R. The Deutsches Elektronen-Synchrotron DESY is acknowledged for the provision of beamtime at P07 and P07B beamline of the Petra III synchrotron radiation facility under the project I-20170054 EC.

Conflicts of Interest: The authors declare no conflict of interest.

References

1. Inoue, A.; Kawamura, Y.; Matsushita, M.; Hayashi, K.; Koike, J. Novel hexagonal structure and ultrahigh strength of magnesium solid solution in the Mg–Zn–Y system. *J. Mater. Res.* **2001**, *16*, 1894–1900. [CrossRef]
2. Yamasaki, M.; Hashimoto, K.; Hagihara, K.; Kawamura, Y. Effect of multimodal microstructure evolution on mechanical properties of Mg–Zn–Y extruded alloy. *Acta Mater.* **2011**, *59*, 3646–3658. [CrossRef]
3. Oñorbe, E.; Garcés, G.; Pérez, P.; Adeva, P. Effect of the LPSO volume fraction on the microstructure and mechanical properties of Mg–Y2X–ZnX alloys. *J. Mater. Sci.* **2012**, *47*, 1085–1093. [CrossRef]
4. Yamasaki, M.; Anan, T.; Yoshimoto, S.; Kawamura, Y. Mechanical properties of warm-extruded Mg–Zn–Gd alloy with coherent 14H long periodic stacking ordered structure precipitate. *Scr. Mater.* **2005**, *53*, 799–803. [CrossRef]
5. Honma, T.; Ohkubo, T.; Kamado, S.; Hono, K. Effect of Zn additions on the age-hardening of Mg–2. *0Gd–1.2Y–0.2Zr alloys Acta Mater.* **2007**, *55*, 4137–4150.
6. Homma, T.; Kunito, N.; Kamado, S. Fabrication of extraordinary high-strength magnesium alloy by hot extrusion. *Scr. Mater.* **2009**, *61*, 644–647.
7. Xu, C.; Zheng, M.Y.; Xu, S.W.; Wu, K.; Wang, E.D.; Kamado, S.; Wang, G.J.; Lu, X.Y. Ultra high-strength Mg-Gd-Y-Zn-Zr alloy sheets processed by large-strain hot rolling and ageing. *Mater. Sci. Eng. A* **2012**, *547*, 93–98. [CrossRef]
8. Xu, C.; Zheng, M.; Xu, S.; Wu, K.; Wang, E.; Fan, G.; Kamado, S. Improving strength and ductility of Mg-Gd-Y-Zn-Zr alloy simultaneously via extrusion, hot rolling and ageing. *Mater. Sci. Eng. A* **2015**, *643*, 137–141. [CrossRef]
9. Xu, C.; Fan, G.H.; Nakata, T.; Liang, X.; Chi, Y.Q.; Qiao, X.G.; Cao, G.J.; Zhang, T.T.; Huang, M.; Miao, K.S.; et al. Deformation behaviour of ultra-strong and ductile Mg-Gd-Y-Zn-Zr alloy with bimodal microstructure. *Metall. Mater. Trans. A* **2018**, *49*, 1931–1947. [CrossRef]

10. Xu, C.; Nakata, T.; Qiao, X.; Zheng, M.; Wu, K.; Kamado, S. Effect of LPSO and SFs on microstructure evolution and mechanical properties of Mg-Gd-Y-Zn-Zr alloy. *Sci. Rep.* **2017**, *7*, 40846. [CrossRef] [PubMed]
11. Shao, J.; Chen, Z.; Chen, T.; Wang, R.; Liu, Y.; Liu, C. Texture evolution, deformation mechanism and mechanical properties of the hot rolled Mg-Gd-Y-Zn-Zr alloy containing LPSO phase. *Mater. Sci. Eng. A* **2018**, *731*, 479–486. [CrossRef]
12. Sun, W.T.; Qiao, X.G.; Zheng, M.Y.; Zhao, X.J.; Chen, H.W.; Gao, N.; Starink, M.J. Achieving ultra-high hardness of nanostructures Mg-8.2Gd-3.2Y-1.0Zn-0.4Zr alloy produced by a combination of high pressure torsion and ageing treatment. *Scr. Mater.* **2018**, *155*, 21–25. [CrossRef]
13. Sun, W.T.; Qiao, X.G.; Zheng, M.Y.; Xu, C.; Kamado, S.; Zhao, X.J.; Chen, H.W.; Gao, N.; Starink, M.J. Altered ageing behaviour of a nanostructured Mg-8.2Gd-3.8Y-1.0Zn-0.4Zr alloy processed by high pressure torsion. *Acta Mater.* **2018**, *151*, 260–270. [CrossRef]
14. Garces, G.; Muñoz-Morris, M.A.; Morris, D.G.; Perez, P.; Adeva, P. Optimization of strength by microstructural refinement of MgY2Zn1 alloy during extrusion and ECAP processing. *Mater. Sci. Eng. A* **2014**, *614*, 96–105. [CrossRef]
15. Garcés, G.; Muñoz-Morris, M.A.; Morris, D.G.; Perez, P.; Adeva, P. Maintaining high strength at high temperature in a Mg-Y-Zn-Gd alloy by heat treatments and severe deformation processing. *Metall. Mater. Trans. A* **2015**, *46*, 5644–5655. [CrossRef]
16. Hammersley, A.P. *FIT2D: An Introduction and Overview*; ESRF Internal Report ESRF97HA02T; European Synchrotron Radiation Source: Grenoble, France, 1997.
17. Oñorbe, E.; Garcés, G.; Dobes, F.; Pérez, P.; Adeva, P. High-temperature mechanical behavior of extruded Mg-Y-Zn alloy containing LPSO phases. *Metall. Mater. Trans. A* **2013**, *44*, 2869–2883. [CrossRef]
18. Garcés, G.; Cabeza, S.; Barea, R.; Pérez, P.; Adeva, P. Maintaining high strength in Mg-LPSO alloys with low yttrium content using severe plastic deformation. *Materials* **2018**, *11*, 733. [CrossRef]
19. Tane, M.; Nagai, Y.; Kimizuka, H.; Hagihara, K.; Kawamura, Y. Elastic properties of an Mg-Zn-Y alloy single crystal with a long-period stacking-ordered structure. *Acta Mater.* **2013**, *61*, 6338–6351. [CrossRef]
20. Oñorbe, E.; Garcés, G.; Pérez, P.; Cabezas, S.; Klaus, M.; Genzel, C.; Frutos, E.; Adeva, P. The evolution of internal strain in Mg–Y–Zn alloys with a long period stacking ordered structure. *Scr. Mater.* **2011**, *65*, 719–722. [CrossRef]
21. Garces, G.; Morris, D.G.; Muñoz-Morris, M.A.; Perez, P.; Tolnai, D.; Mendis, C.; Stark, A.; Lim, H.K.; Kim, S.; Schell, N.; et al. Plasticity analysis by synchrotron radiation in a Mg97Y2Zn1 alloy with bimodal grain structure and containing LPSO phase. *Acta Mater.* **2015**, *94*, 78–86. [CrossRef]
22. Garces, G.; Perez, P.; Cabeza, S.; Kabra, S.; Gan, W.; Adeva, P. Effect of extrusion temperature on the plastic deformation of an Mg-Y-Zn alloy containing LPSO phase using in situ neutron diffraction. *Metall. Mater. Trans. A* **2017**, *48*, 5332–5343. [CrossRef]
23. Hagihara, K.; Yokotani, N.; Umakoshi, Y. Plastic deformation behavior of Mg12YZn with 18R long-period stacking ordered structure. *Intermetallics* **2010**, *18*, 267–276. [CrossRef]
24. Garces, G.; Munoz-Morris, M.A.; Morris, D.G.; Jimenez, J.A.; Perez, P.; Adeva, P. The role of extrusion texture on strength and its anisotropy in a Mg-base alloy composed of the Long-Period-Structural-Order phase. *Intermetallics* **2014**, *55*, 167–176. [CrossRef]
25. Garcés, G.; Máthis, K.; Medina, J.; Horváth, K.; Drozdenko, D.; Oñorbe, E.; Dobroň, P.; Pérez, P.; Klaus, M.; Adeva, P. Combination of in-situ diffraction experiments and acoustic emission testing to understand the compression behavior of Mg-Y-Zn alloys containing LPSO phase under different loading conditions. *Int. J. Plast.* **2018**, *106*, 107–128. [CrossRef]